# Increasing the Power of Shape Descriptor Based Object Analysis Techniques

Joviša Žunić, Paul L. Rosin, Mehmet Ali Aktaş

**Abstract** An advantage of shape based techniques, for object analysis tasks, is that shape allows a large number of numerical characterizations. Some of these have an intuitively clear meaning, while others do not, but they are still very useful because they satisfy some desirable properties (e.g. invariance with respect to a set of certain transformations). In this chapter we focus on numerical shape characteristics that have a clear intuitive interpretation – i.e. based on such numerical values, we can predict, to some extent, what the considered object looks like. This is beneficial, since it enables a priori appraisal of whether certain shape characteristics have suitable discriminative potential that make them appropriate for the intended task. By their nature, the number of such methods cannot be as large as the number of methods to allocate shape/object characteristics based on some formalism (algebraic, geometric, probabilistic, etc). Because of that, some other possibilities to increase the discriminative capacity of the methods based on numerical shape characteristics, with an intuitively predictable meaning, are considered. Herein, we observe two such possibilities: the use of tuning parameters to obtain a family of shape characteristics, and the use of multiple shapes derived from the objects analyzed.

Joviša Žunić
Mathematical Institute, Serbian Academy of Sciences and Arts, Belgrade, Serbia
e-mail: jovisa_zunic@mi.sanu.ac.rs

Paul L. Rosin
School of Computer Science & Informatics, Cardiff University, Cardiff, CF24 3AA, UK
e-mail: Paul.Rosin@cs.cardiff.ac.uk

Mehmet Ali Aktaş
Computer Science, Toros University, Turkey.
e-mail: mehmet.aktas@toros.edu.tr

## 1 Introduction

Shape is an important component of the human visual system, and is also widely used in computer vision to provide a means of describing objects as a precursor to identifying them. If object boundaries can be reliably extracted (which of course remains a challenge for unconstrained scenes, but is achievable in many other cases) then shape descriptors offer many advantages to those based on intensity, colour, texture, etc. First, although those latter approaches incorporate more information, offering a richer descriptive power, they are consequently also more sensitive to potentially irrelevant variations in illumination, colouring, etc. For instance, whereas the shape of a typical car is clear cut, cars come in many colours, and so colour (unlike shape) is not helpful to the task of assigning an object to the general class of cars. Second, most shape descriptors can be easily normalised so that they are invariant to many transformations (e.g. translation, rotation, scaling, shearing) without requiring expensive and less reliable methods such as scale-space based image processing. Third, many techniques for shape based analysis provide a compact descriptor, that is not only efficient to store, but is also well suited to efficient matching.

Many shape properties, herein called *shape descriptors*, are known to be very suitable for a numerical evaluation (e.g. shape convexity, ellipticity, elongation, compactness, linearity, sigmoidality, tortuosity, etc.). Methods developed to evaluate a certain shape descriptor will be called *shape measures*. Examples of shape measures already developed are: convexity [26, 32, 45], circularity [15, 24, 30, 43], compactness [17], linearity [10, 36, 41], ellipticity [1, 29, 38, 42, 24], sigmoidality [31], rectilinearity [44], tortuosity [12], and many more. As it can be seen, there are shape descriptors with multiple measures developed for their numerical evaluation. This is because none of the shape measures are ideally suited for all the possible applications.

Apart from the shape measures mentioned, which relate to a certain shape property, there are generic shape measures which are not originally designed to measure a specific shape property/characteristic. Among them are: Fourier descriptors [5, 39], moment invariants [16, 20], shape-illumination invariants [3], and so on. Those measures satisfy some desirable properties (e.g. invariance with respect to some transformations) and their power comes from the fact that, at least in theory, an infinite number of them can be generated and assigned to a given object/shape. A drawback is that their behavior is not well explained and cannot be predicted. This further implies that their suitability for a certain task has to be verified through an intensive experimental study, which is always a time consuming process.

Contrary to the generic shape measures, the measures which do relate to a certain shape property have a well understood and predictable behavior. Their disadvantage is that their number is limited. This further causes a limited discriminative power of the object analysis tools based on such measures, particularly when dealing with huge data sets. In this chapter we consider possibilities of increasing the discriminative power of such tools, with applications in image processing and computer vision tasks. We discuss the following possibilities: (i) An involvement of a tuning parameter; (ii) Allocation of multiple shapes to the objects considered; (iii) A combination

of the approaches in (i) and (ii). Our discussion is supported with experimental results.

Throughout this chapter we will assume that all occurring shapes are bounded. In order to avoid discussions on pathological situations, we will say that two shapes are equal if their set differences have area equal to zero. This is obviously not a restriction in practical applications – e.g. a closed ellipse $\{(x,y) \mid x^2+3\cdot y^2 \leq 1\}$ and the "open" one $\{(x,y) \mid x^2+3\cdot y^2 < 1\}$ are considered to be the same shape.

The geometric moment $m_{p,q}(S)$ of a given shape $S$, represented by a planar bounded region, is defined as

$$m_{p,q}(S) \;=\; \iint_S x^p\, y^q\, dx\, dy. \tag{1}$$

Obviously, $m_{0,0}(S)$ equals the area of $S$. As a short reminder, the centroid of a given shape $S$ is defined as

$$\left(\frac{\iint_S x\, dx\, dy}{\iint_S dx\, dy},\; \frac{\iint_S y\, dx\, dy}{\iint_S dx\, dy}\right) \;=\; \left(\frac{m_{1,0}(S)}{m_{0,0}(S)},\; \frac{m_{0,1}(S)}{m_{0,0}(S)}\right). \tag{2}$$

Since shape does not change under the translations, we will assume that all the appearing shapes are positioned such that their centroid coincides with the origin. In other words:

$$m_{1,0}(S) \;=\; \iint_S x\, dx\, dy \;=\; 0 \qquad \text{and} \qquad m_{0,1}(S) \;=\; \iint_S y\, dx\, dy \;=\; 0 \tag{3}$$

will be assumed, even if not mentioned, for all the shapes considered.

Finally, $S(\omega)$ will denote the shape $S$ rotated around its centroid by the angle $\omega$.

## 2 Power Increase by Introducing a Tuning Parameter

In this section we discuss a family of circularity measures, introduced as a generalization of the first Hu moment invariant [16], by incorporating one parameter [43]. The role of this introduced parameter is to control the behavior of the circularity measures from the given family. Shape interpretation of the first Hu moment invariant, $I_1(S)$,

$$I_1(S) \;=\; \iint_S (x^2+y^2)\, dx\, dy \tag{4}$$

has been analyzed in [43]. It has been shown that the first Hu moment invariant, $I_1(S)$, ranges over the interval $[\frac{1}{2\pi},\infty)$ and returns the minimum possible value $\frac{1}{2\pi}$ for circles only. This property has been used to define the new circularity measure, $\mathscr{C}(S)$, for planar shapes:

$$\mathscr{C}(S) \;=\; \frac{1}{2\pi}\cdot\frac{m_{0,0}(S)^2}{m_{2,0}(S)+m_{0,2}(S)} \;=\; \frac{1}{2\cdot\pi\cdot I_1(S)}. \tag{5}$$

Such a circularity measure $\mathscr{C}(S)$ ranges over the interval $(0,1]$, produces the value 1 if and only if the considered shape $S$ is a circle, and is invariant with respect to translation, rotation, and scaling transformations. It also might be said that the new circularity measure fits well with our perception of what a circularity measure should be – a quantity which indicates how much a shape given differs from a circle. Shapes with relatively large $\mathscr{C}(S)$ values are nearly circular, while shapes with small $\mathscr{C}(S)$ values have a nearly linear structure. We illustrate this by a small collection of fish shapes and their assigned circularity values, but more examples can be found in [43]. Five fish shapes are listed in Fig.1, in accordance with their computed $\mathscr{C}(S)$

0.9579 0.8755 0.4506 0.3361 0.1390

**Fig. 1** Fish shapes are ranked with respect to their computed $\mathscr{C}(S)$ circularity values.

circularity values. The largest circularity 0.9579 is assigned to the shape on the left, which is as expected since this shape is nearly circular. The smallest circularity value 0.1390 is assigned to the shape on the right. Again, such a small circularity comes from the fact that this shape has a nearly linear structure. Our judgment is that we may say that these values, as well as the remaining three values, and the ranking obtained, are in accordance with human perception.

The circularity measure $\mathscr{C}(S)$ is area based, and because of this is robust, i.e. relatively resistant to small shape deformations or to defects caused by noise, for example. Of course, such a (robustness) property is an advantage in many situations but it could be a disadvantage in situations when high precision is required. To avoid such a possible drawback, the measure $\mathscr{C}(S)$ has been modified. A tuning parameter $\alpha$ was introduced [43] to produce a family of circularity measures $\mathscr{C}_\alpha(S)$ as follows:

$$\mathscr{C}_\alpha(S) \;=\; \frac{1}{(\alpha+1)\cdot\pi^\alpha}\cdot\frac{m_{0,0}(S)^{\alpha+1}}{\iint_S (x^2+y^2)^\alpha dxdy} \tag{6}$$

for all $\alpha > 0$[1] and for all bounded compact planar shapes $S$. Obviously, the measure $\mathscr{C}(S)$ also belongs to the new family of circularity measures defined in (6), since $\mathscr{C}(S) = \mathscr{C}_{\alpha=1}(S)$. All circularity measures from the family $\mathscr{C}_\alpha(S)$ keep the basic desirable properties. They range over $(0,1]$, with the equality $\mathscr{C}_\alpha(S) = 1$ satisfied for circles only. Measures $\mathscr{C}_\alpha(S)$ are invariant with respect to similarity transformations as well. The main role of the tuning parameter $\alpha$ is to enable control of the sensitivity/robustness properties of $\mathscr{C}_\alpha(S)$. It has been shown that bigger values of $\alpha$ lead to a more sensitive measure $\mathscr{C}_\alpha(S)$. More detailed discussion can be found

[1] For an extension to the circularity measures with $\alpha \in (-1,0)$, see [43].

in [43], but here we give a lemma which supports the previous statement. Indeed, Lemma 1 says that for any shape $S$ different from a circle, there is a parameter $\alpha$ such that $\mathscr{C}_\alpha(S)$ is arbitrarily close to 0. In other words, there is a choice of circularity measure $\mathscr{C}_\alpha(S)$ (i.e. the choice of the parameter $\alpha$) which would penalize, strongly enough, any existing difference between the shape $S$ and a circle.

**Lemma 1.** *For a bounded planar compact shape $S$, different from a circle, the following equality is true*

$$\lim_{\alpha\to\infty} \mathscr{C}_\alpha(S) \;=\; 0. \tag{7}$$

Some of the benefits from having the possibility to tune the behavior of circularity measures are illustrated by examples in Fig.2. All the four shapes listed can be understood as very similar to a circle. The first shape is a regular 7-gon while the remaining three shapes are obtained from a circle by adding noise. For the second and third shape a different level noise is added to the shape boundary, while salt noise (i.e. holes) is added to the interior of the fourth shape. The circularity $\mathscr{C}(S)$ of all these shapes is very close to 1, and $\mathscr{C}(S)$ can neither distinguish among these shapes nor detect the presence of the obvious irregularities. These irregularities become visible once measures $\mathscr{C}_\alpha(S)$ from the new family are employed. Indeed, looking at the

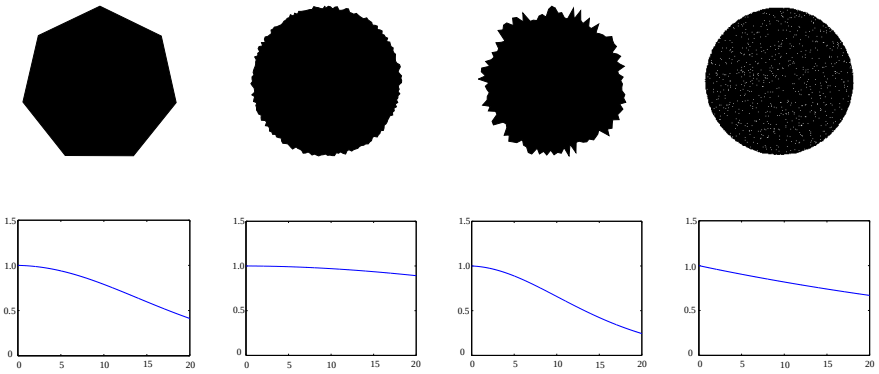


**Fig. 2** Graphs of the measured circularities $\mathscr{C}_\alpha(S)$, for $\alpha \in [0,20]$, are given below the corresponding shapes.

graphs of $\mathscr{C}_\alpha(S)$ (considered as a function in $\alpha$), displayed in the second row in Fig.2, we see that an increase of $\alpha$ leads to a decrease of $\mathscr{C}_\alpha(S)$. After some point, it becomes clearly evident that all the given shapes differ from a circle, and also that each of these shapes differs from the others. For example, if we set $\alpha = 20$ then, for all the shapes displayed, the computed $\mathscr{C}_\alpha(S)$ circularities are all mutually different.

Next, we illustrate that some classification accuracies, reached by some of the well known shape measures, can be outperformed by selecting a suitable measure from the family $\mathscr{C}_\alpha(S)$. For this purpose we will use the standard circularity measure, and the circularity measures of Proffitt [24] and Haralick [15]. The standard

circularity measure $\mathscr{C}_{st}(S)$ exploits the fact that among all shapes with the same perimeter, the circle has the largest area. It is defined as

$$\mathscr{C}_{st}(S) = \frac{4 \cdot \pi \cdot Area\_of\_S}{(Perimeter\_of\_S)^2}. \tag{8}$$

Note that in the following experiments the perimeter of $S$ was calculated for $\mathscr{C}_{st}(S)$ either directly from the pixel boundaries extracted from the images with inter-pixel weights set according to Dorst and Smeulders [8], or alternatively the perimeters were calculated from polygonal approximations of the boundaries [25]. For classification, leave one out testing was performed with a nearest neighbor classifier using Euclidean distances.

| circularity measure | mammography | | |
|---|---|---|---|
| | circ./spic. | mal./ben. | 4 groups |
| $\mathscr{C}_{\alpha=1/8}(S)$ | 83.33 | 66.67 | 51.85 |
| $\mathscr{C}_{\alpha=1/4}(S)$ | 85.19 | 64.81 | 51.85 |
| $\mathscr{C}_{\alpha=1/2}(S)$ | 75.93 | 57.41 | 42.59 |
| $\mathscr{C}_{\alpha=1}(S)$ | 68.52 | 68.52 | 51.85 |
| $\mathscr{C}_{\alpha=2}(S)$ | 75.93 | 68.52 | 53.70 |
| $\mathscr{C}_{\alpha=4}(S)$ | 72.22 | 46.30 | 33.33 |
| $\mathscr{C}_{\alpha=8}(S)$ | 79.63 | 59.26 | 50.00 |
| $\mathscr{C}_{\alpha=16}(S)$ | 87.04 | 57.41 | 51.85 |
| $\mathscr{C}_{\alpha=32}(S)$ | **90.74** | **70.37** | **64.81** |
| $\mathscr{C}_{st}(S)$ pixel | 87.04 | 59.26 | 57.41 |
| $\mathscr{C}_{st}(S)$ polygon | 85.19 | 59.26 | 57.41 |
| Haralick [15] | 68.52 | 46.30 | 37.04 |
| Proffitt [24] | 51.85 | 42.59 | 25.93 |

**Table 1** Applications of the circularity measures to: classification of mammographic masses. The classification accuracies, for three classification tasks, are given for different choices of the circularity measures. The best performing measure was $\mathscr{C}_{\alpha=32}(S)$ (the score highlighted in bold).

For this example, circularity was measured for the set of 54 masses from mammograms, combining images from the MIAS and Screen Test databases [27], see Fig.3. Rangayyan *et al.* [27] assessed the measures by classifying them as circumscribed/spiculated, benign/malignant, and CB/CM/SB/SM, in two group and four group classification experiments. Their best shape measure results for the three classification tasks were: (i) circumscribed versus spiculated: 88.9% achieved by both $\mathscr{C}_{st}(S)$ and a Fourier based shape factor, (ii) benign versus malignant: 75.9% achieved by the Fourier based shape factor, (iii) four-way discrimination: 64.8% achieved by both $\mathscr{C}_{st}(S)$ and the Fourier based shape factor.[2] From Table 1 we see that the best results from using $\mathscr{C}_{\alpha}(S)$ occurred for $\alpha = 32$ and were respectively

[2] We note that our results for $\mathscr{C}_{st}(S)$ listed in Table 1 do not match Rangayyan *et al.*'s [27] reported accuracies for $\mathscr{C}_{st}(S)$. This can be attributed to several factors: (i) different classifiers were used, and also (ii) different methods for estimating perimeter may have been used.

better, worse, and equal to Rangayyan *et al.*'s. The other circularity measures did not perform as well as $\mathscr{C}_\alpha(S)$.

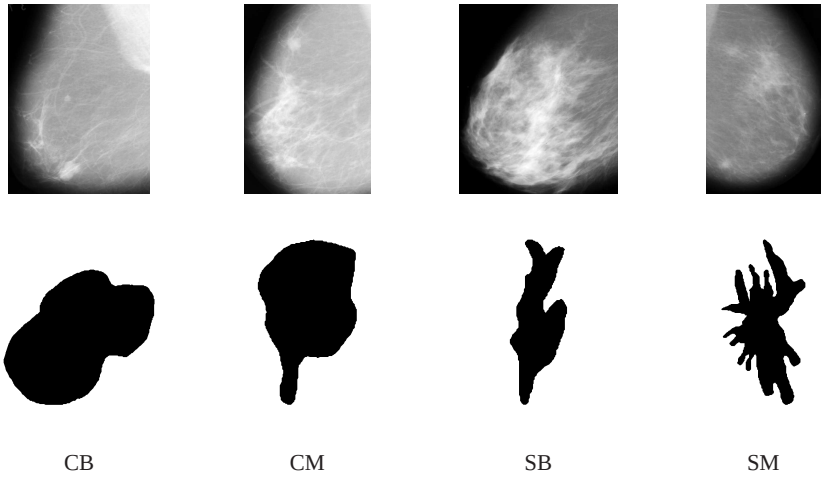


**Fig. 3** Examples of the four classes of mammographic masses: circumscribed benign (CB), circumscribed malignant (CM), spiculated benign (SB), spiculated malignant (SM). The masses were extracted from the mammograms (top row), and have been drawn rescaled (bottom row).

## 3 Family of Ellipticity Measures with an Application in an Galaxy Classification Task

Shape ellipticity measures are intensively studied in the literature. An early attempt [38] goes back to 1910. Notice that there are two approaches for how to measure shape ellipticity. The first one assumes that all ellipses are of the same shape, regardless of their axis length ratios, e.g. [1, 29]. Another approach assumes that ellipses whose axis ratios differ also differ in shape, e.g. [2]. It is not possible to say a priori which approach is better. In some applications the first approach would be more appropriate, whilst in some others the second is preferred.

Ellipticity measures considered in this section, from the family introduced recently [2], assume that ellipses with a different axis length ratio are different in shape. A precise definition follows.

**Definition 1.** Let a bounded planar shape $S$, whose centroid coincides with the origin, be given. For every $\rho \in (0,1]$ the ellipticity measure $\mathscr{E}_\rho(S)$ of $S$, is defined as

$$\mathscr{E}_\rho(S) \;=\; \frac{1}{2\cdot\pi}\cdot\frac{m_{0,0}(S)^4}{\min\limits_{\omega\in[0,2\pi]}\iint_{S(\omega)}\left(\frac{x^2}{\rho}+\rho\cdot y^2\right)\,dx\,dy}. \tag{9}$$

*Note 1.* The formula in (9) enables an easy and straightforward numerical computation of $\mathscr{E}_\rho(S)$, with $\rho\in(0,1]$. There is also a closed formula for the computation of $\mathscr{E}_\rho(S)$, derived recently in [40].

All the ellipticity measures $\mathscr{E}_\rho(S)$, from Definition 1 have the following properties (for a proof see [2]):

(a) $\mathscr{E}_\rho(S)\in(0,1]$, for any shape $S$;
(b) $\mathscr{E}_\rho(S)=1$ if and only if $S$ is an ellipse whose axis length ratio is $\rho$;
(c) $\mathscr{E}_\rho(S)$ is invariant with respect to similarity transformations.

Theoretical foundations for understanding the behavior of the new ellipticity measures $\mathscr{E}_\rho(S)$ are established in [2]. Here we give a brief discussion. The parameter $\rho$ can be understood as a tuning parameter, because the behavior of the ellipticity measures, from $\{\mathscr{E}_\rho(S)\mid\rho\in(0,1]\}$, depends on the choice of the parameter $\rho$. For a fixed $\rho$, the measure $\mathscr{E}_\rho(S)$ indicates how much the considered shape $S$ differs from a perfect ellipse $E(\rho)$ whose axes length ratio is $\rho$. The highest score, equal to 1, is given only to the $E(\rho)$ ellipses. For all the shapes different from $E(\rho)$, including the ellipses whose axes length ratio differs from $\rho$, the computed $\mathscr{E}_\rho(S)$ ellipticities are strictly less than 1. Which values of the parameter $\rho$ should be selected depends on the application which is going to be performed. Ellipticity $\mathscr{E}_\rho(S)$, corresponding to one selection of the parameter $\rho$, can perform well in one application, but also can have a poor performance in another.

In this section, in addition to the use of a tunable ellipticity measures, we consider another possibility to increase the discriminative capacity of shape based object analysis tools. The idea is to assign a number of shapes to an object presented in an image, instead of just a single shape, as is the common approach. Multiple shapes can be assigned in several ways (e.g. as it is done in this section – see Fig.5, and also as it is done in Section 4 – see Fig.8, or in [28], etc.). In this section we will assign two shapes to each object by using two versions of Otsu's thresholding method [22]: A "global" one (the same threshold level is applied to all pixels) and a "local" one (the original method is applied to blocks of the original image, so that the threshold level applied varies). This means that we allocate two shapes (represented as two binary images) for each object. For each of these two shapes/images we will compute three shape measures, which will comprise the components of the feature vectors used for classification.

This approach will be applied to a galaxy classification task. The elliptical and spiral galaxies, listed in the Nearby Galaxy Catalog [9], are used as the data/shape set. The same data set has been used by many others, and the classification task has been already recognized as a difficult problem [18]. Many approaches have been applied and used to provide an automatic machine galaxy classification, e.g. neural

networks approaches [4, 14, 21], fuzzy sets theory [19], geometric shape features [11, 13], shape squareness [34], fractal signatures [18], etc.

The benchmark results, prior to a 100% classification rate obtained in [2], were 92.3% and 95.1%, obtained in [18] by using nearest neighbor and neural network classifiers, respectively.

### *3.1 Ellipticity Measures Used and Classification Results Obtained*

Three ellipticity measures were used to perform the galaxy classification task. Two of them are from the family $\mathscr{E}_\rho(S)$:

- $$\mathscr{E}_{\rho=0.7}(S) = \frac{1}{2\cdot\pi}\cdot\frac{m_{0,0}(S)^4}{\min\limits_{\omega\in[0,2\pi]}\iint_{S(\omega)}\left(\frac{x^2}{0.7}+0.7\cdot y^2\right)\,dx\,dy} \qquad (\mathbf{m1})$$

- $$\mathscr{E}_{\rho=0.9}(S) = \frac{1}{2\cdot\pi}\cdot\frac{m_{0,0}(S)^4}{\min\limits_{\omega\in[0,2\pi]}\iint_{S(\omega)}\left(\frac{x^2}{0.9}+0.9\cdot y^2\right)\,dx\,dy} \qquad (\mathbf{m2})$$

while the third ellipticity measure used is introduced in [1] and is defined as follows

- $$\mathscr{E}(S) = \frac{1}{2\cdot\pi}\cdot\frac{m_{0,0}(S)^4}{\min\limits_{\omega\in[0,2\pi]}\iint_{S(\omega)}\left(\frac{x^2}{\gamma}+\gamma\cdot y^2\right)\,dx\,dy} \qquad (\mathbf{m3})$$

  where the parameter $\gamma$ is defined as

$$\gamma = \frac{\sqrt{\mu_{2,0}(S)+\mu_{0,2}(S)+\sqrt{4\cdot(\mu_{1,1}(S))^2+(\mu_{2,0}(S)-\mu_{0,2}(S))^2}}}{\sqrt{\mu_{2,0}(S)+\mu_{0,2}(S)-\sqrt{4\cdot(\mu_{1,1}(S))^2+(\mu_{2,0}(S)-\mu_{0,2}(S))^2}}}.$$

Ellipticity measures $\mathscr{E}_{\rho=0.7}(S)$ and $\mathscr{E}_{\rho=0.9}(S)$ were selected according to the graphs displayed in Fig.4. Precisely, 32 shapes were selected randomly and then thresholded by both the global and local methods. The graphs of $\mathscr{E}_\rho(S)$, for $\rho$ varying through the interval $(0,1]$, were computed. The graphs of $\mathscr{E}_\rho(S)$ corresponding to shapes obtained by the global thresholding are on the left in Fig.4, while the graphs $\mathscr{E}_\rho(S)$ for shapes obtained by the local thresholding are on the right in Fig.4. Our hypothesis was: "Since for both $\rho = 0.7$ and $\rho = 0.9$ the values of $\mathscr{E}_\rho(S)$ are "scattered" reasonably well, an efficient discrimination among the galaxy shapes would be enabled by using the functions/measures $\mathscr{E}_{\rho=0.7}(S)$ and $\mathscr{E}_{\rho=0.9}(S)$". Also, the selected parameters are preferred to be reasonably different. It turns out that, at least in this case, the hypothesis was valid.

Thus, each galaxy **g** was represented by a 6-dimensional feature vector determined as follows:

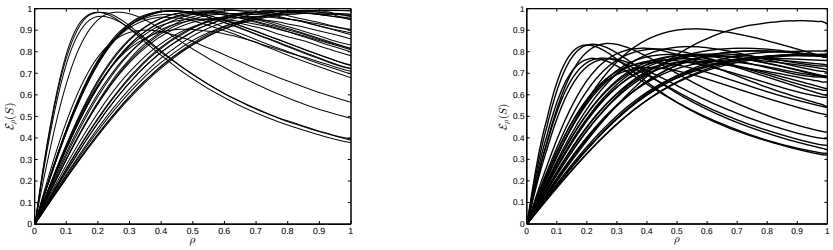

**Fig. 4** $\mathscr{E}_\rho(S)$, $\rho \in (0,1]$, graphs for the shapes $S$ obtained by thresholding of 32 randomly selected galaxy images: global thresholding applied (on the left) and local thresholding applied (on the right).

$$\left(\mathscr{E}_{\rho=0.7}(S'_{\mathbf{g}}),\ \mathscr{E}_{\rho=0.9}(S'_{\mathbf{g}}),\ \mathscr{E}(S'_{\mathbf{g}}),\ \mathscr{E}_{\rho=0.7}(S''_{\mathbf{g}}),\ \mathscr{E}_{\rho=0.9}(S''_{\mathbf{g}}),\ \mathscr{E}(S''_{\mathbf{g}})\right) \qquad (10)$$

where $S'_{\mathbf{g}}$ and $S''_{\mathbf{g}}$ are the shapes (i.e. binary images) obtained from the original image (of the galaxy **g**) thresholded by two selected methods (the global and local one). Some examples are in Fig.5: original images are in the left column, shapes $S'_{\mathbf{g}}$ obtained by the global thresholding are in the middle column, while shapes $S''_{\mathbf{g}}$ obtained by local thresholding are in the right column.

We have used the $k$-Nearest Neighbour Classifier ($k$-NN), with $k = 5$. For the training set we have used 4 elliptical and 28 spiral galaxies (e.g. approximately 30% of the galaxies have been used for the training – the same percentage as in [18]). The classification was performed on the complete data set (galaxies selected for the training were also included). In order to get a reliable indicator about the efficiency of the classification "mechanism" described above, 100 experiments were performed. The experiments were mutually independent – i.e. galaxies for the training set (4 elliptical and 28 spiral galaxies) have been selected randomly in every experiment.

The classification results were very good, and outperform the previous accuracies. Among 100 experiments performed, the classification rate of 100% was achieved 3 times. The average classification rate was 95.6% – better than both best rates obtained by $k$-NN and neural network classifiers in [18]. The minimal classification rate of 90.2% was obtained 4 times. The classification results, for each of the 100 experiments, are displayed in Fig.6. It is worth mentioning that because the ellipticity measures have predictable behavior, it was expected that good classification results might be expected (galaxy shapes have an elliptical structure). Such a prediction would not be possible if some generic shape measures were used instead. The additional tool which led to the maximum classification is the use of multiple shapes assigned to an object/image. To illustrate the latter statement we provide the classification results in experiments where a single shape is allocated to each galaxy. The same ellipticity measures: $\mathscr{E}_{\rho=0.7}(S)$, $\mathscr{E}_{\rho=0.9}(S)$, and $\mathscr{E}(S)$ were used again. As expected, smaller classification rates were obtained. The classification results, based on 100 mutually independent experiments, are displayed in Fig.7. As it can be seen:

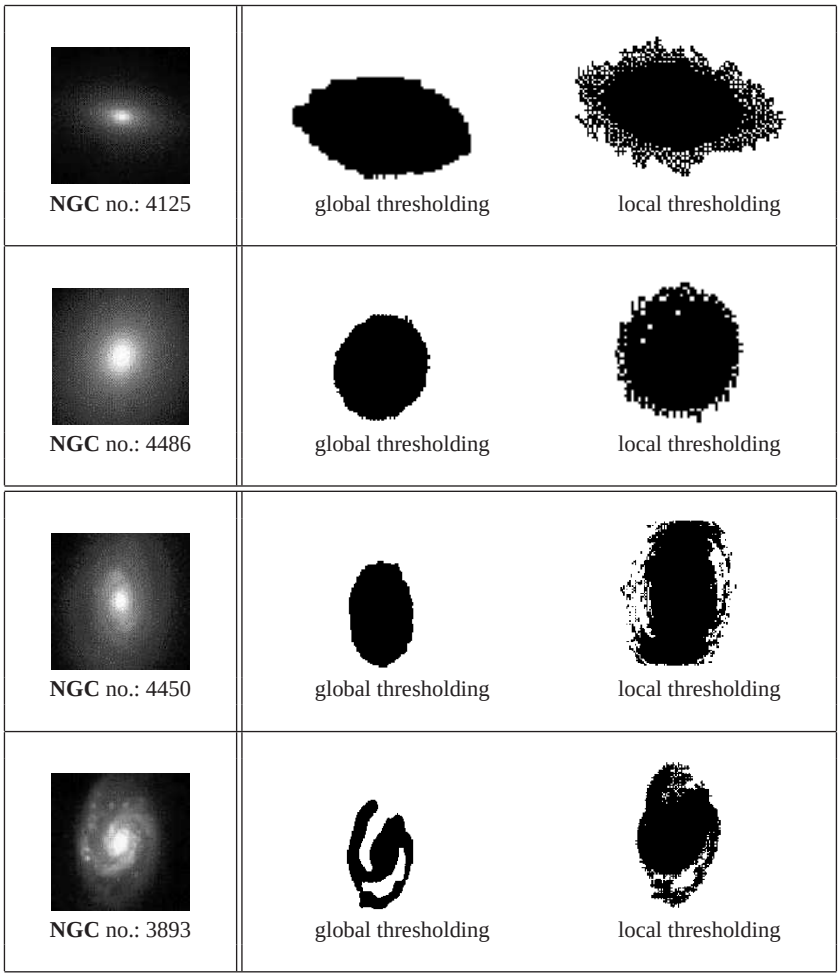


**Fig. 5** Original images and their **NGC** number are in the left column; shapes obtained by the global and local thresholding are in the middle and right column, respectively.

- If the shapes obtained by the global thresholding and the 3-dimensional feature vector

$$\left(\mathscr{E}_{\rho=0.7}(S'_{\mathbf{g}}),\ \mathscr{E}_{\rho=0.9}(S'_{\mathbf{g}}),\ \mathscr{E}(S'_{\mathbf{g}})\right) \tag{11}$$

  were used, the following rates were achieved:

  – the average classification rate: 87.5%;
  – the maximum classification rate: 92.1%;
  – the minimal classification rate: 82.4%.

- If single shapes, obtained by the local thresholding method, and the 3-dimensional feature vector

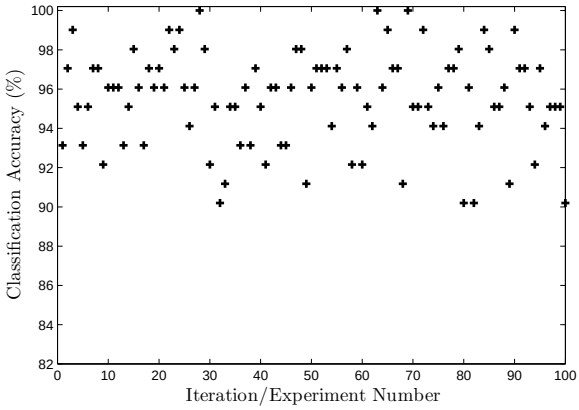


**Fig. 6** Classification rates obtained for 100 mutually independent galaxy classification experiments.

$$\left(\mathscr{E}_{\rho=0.7}(S''_{\mathbf{g}}),\ \mathscr{E}_{\rho=0.9}(S''_{\mathbf{g}}),\ \mathscr{E}(S''_{\mathbf{g}})\right) \tag{12}$$

were used, then the following rates were achieved:

- the average classification rate: 92.2%;
- the maximum classification rate: 96.0%;
- the minimal classification rate: 84.3%.

## 4 Multiple Shapes Assigned to Boundary Simplification

A final pair of experiments is described in which multiple shapes will be derived for each object. Distinct from the experiments in Sections 2 and 3, classification will be performed using boundary based features. Therefore boundary based methods will be employed to generate multiple shapes. This is the most straightforward and appropriate approach if the input data consists of boundaries, and also ensures that the number of components does not change, that open curves remain open, etc.

Our approach to generate multiple shapes from the given data is to perform simplification of the input shapes. This can be applied at different degrees to create an arbitrary number of additional shapes. For the two examples described in this section two approaches are taken: Gaussian blurring and polygonal approximation.

Unlike the previous examples, only boundary information is provided, and there is no additional information such as object intensities. This means that the additional shapes generated will not introduce new information, although there is still a potential benefit to be gained by making different aspects of the data more explicit,

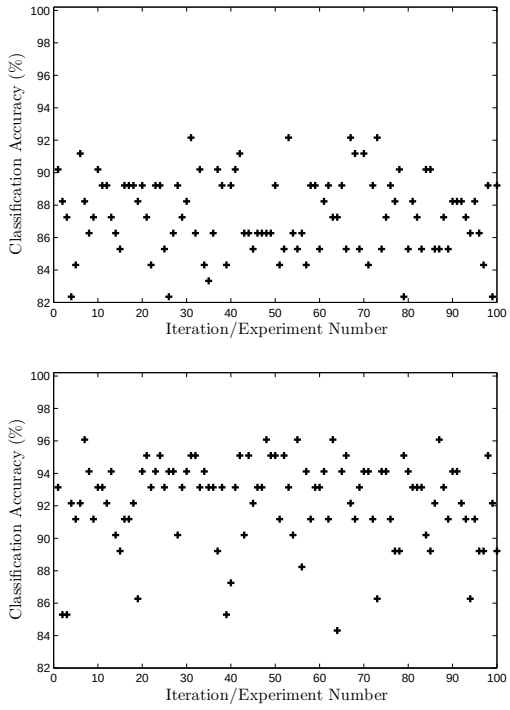


**Fig. 7** Classification rates obtained for 100 mutually independent, simplified classification experiments. Top row: the global thresholding method and the feature vector (11) are used. Bottom row: the local thresholding method and the feature vector (12) are used.

whilst suppressing others. Nevertheless, the expected performance gain is likely to be less than in Section 3.

## *4.1 Closed Curves Example: MPEG-7 CE-1*

In [34] a set of five shape based features (namely, a Fourier based triangularity measure [5], roundness based on the ratio of the areas of the shape and its circumscribing circle, rectangularity based on the ratio of the areas of the shape $S$ and its minimum bounding rectangle, ellipticity based on the first affine moment invariant [29] and convexity based on the areas of the shape and its convex hull) along with two squareness measures ($\mathscr{Q}_{\beta=2}(S)$ and $\mathscr{Q}_{fit}(S)$) were combined to achieve a bull's eye test score of 74.74% when applied to the MPEG-7 CE-1 set of 1400 shapes using a minimum Mahalanobis distance classifier.

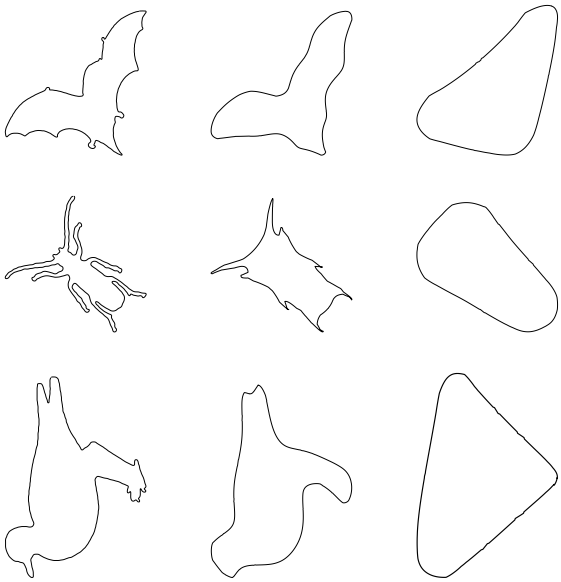

**Fig. 8** Shapes at three levels of smoothing (from left to right: $\{\sigma = 2, 32, 128\}$).

A richer feature set can be obtained by expanding the data set to include multiple smoothed versions of the 1400 curves, and using them to compute additional features. For example, Gaussian blurring was applied at scales $\{\sigma = 2, 32, 128\}$, see some examples in Fig.8. When the additional convexity values produced from these scales was included in the classifier then the test score increased to 75.76%.

## *4.2 Open Curves Example: UJI Pen characters*

The next experiment uses the UJI Pen character data set [6], in which handwriting samples were captured with a stylus. Each of the participating 60 writers wrote two samples of 97 characters, that included ASCII, Spanish and other non-ASCII characters, making up 11640 samples in total. Note that some of the characters are multi-stroke, and that of those, their component strokes do not necessarily touch. The top row in Fig. 9 illustrates some of the different types of characters in the data set, while the middle row demonstrates the wide variability in handwriting styles for a single character. The creators of the data set have split the characters into disjoint training and test sets created by 40 writers and 20 writers respectively.

We used a Support Vector Machine (SVM) to perform classification of the characters: LIBSVM [7] with a Radial Basis Function (RBF) kernel and default settings. Grid search and 5-fold cross validation in the training set were used to obtain the optimized parameters and the model was then applied to the test data.

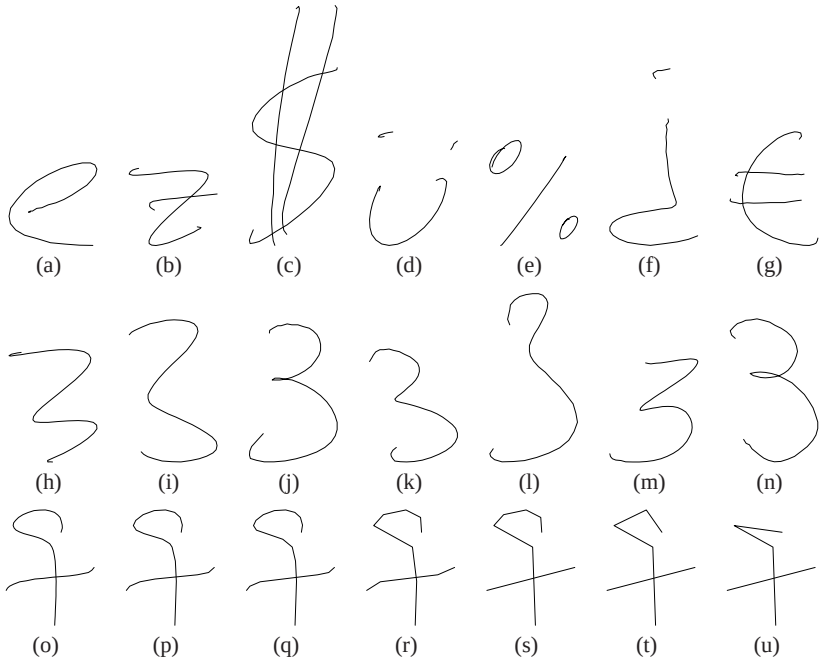


**Fig. 9** Characters from the UJI Pen character data set. *Top row*: a) single simple curve; b) two intersecting curves; c) three intersecting curves; d) three non-intersecting curves; e) a mixture of open and closed curves; f) Spanish character; g) non-ASCII character. *Middle row*: examples showing the variability of a single character across different writers. *Lower row*: one character progressively simplified by increasing degrees of polygonal approximation.

The challenging nature of the data potentially complicates the processes of feature extraction and/or matching, and in the original paper [6] the experiments were restricted to the ASCII alpha-numeric characters, while more recent work has further restricted the task to 26 classes [37]. In our experiments we will use the full set of 97 character classes. The features need to be chosen such that they can be applied to open or closed boundaries comprised of single or multiple components, ruling out many standard shape measures. In our experiments we have used: anisotropy [35], aspect ratio, convexity [46], linearity [33], line moments (both Hu's first seven rotation, translation and scale moment invariants [16] were used as well as six further moment invariants designed for character recognition [23] which are invariant to change in aspect ratio, but are *not* orientation dependent so that e.g. '6' and '9' can be distinguished), rectilinearity [44] (both the regular version $R_1$ and a modification in which the measure is *not* maximized over orientation), and the absolute sum of turning angles.

The classification rate obtained was 51.2% for features extracted from the raw data. Next, the data was simplified using Ramer's polygonal approximation method [25] over a range of scales (distance thresholds of $\{1,2,4,8,16,32,64,128\}$) – see

the bottom row in Fig. 9 for some examples. When classification was performed on the data set using features from any single approximation level then no advantage was found, as the classification rate dropped to 36.40%–50.56%. However, when the features from several scales were combined – namely the raw data, and Ramer thresholds $\{2, 64\}$ – then an increase of classification to 56.67% was achieved. This demonstrates the benefit of augmenting the data set by additional alternative versions of the shapes.

Of course, further improvements could be obtained by developing and using additional features, in particular those specific to the stylus and multi-stroke characteristics of the data. Examples are: trajectories (i.e. temporal information), the number of strokes, the distribution of various stroke characteristics within a character, etc.

## 5 Conclusion

In this chapter we have considered some possibilities to increase the discrimination capabilities of shape based tools used in image processing and computer vision tasks. We focused on shape based characteristics/properties with a intuitively clear meaning. Many of these properties, commonly named shape descriptors, are clearly identified (e.g. convexity, linearity, elongation, circularity, sigmodality, etc.) and methods for their computation (i.e. numerical evaluation/estimation) are derived. These methods are called shape measures. It has been noted that a single method for evaluation of a given shape descriptor does not suit all applications. That is why, for several shape descriptors, multiple shape measures have already been developed. Among them, convexity, circularity, and ellipticity are probably the shape descriptors with the largest number of measures developed for their evaluation. Multiple measures, related to the same descriptors, are used (either alternatively or jointly) as components in the feature vectors allocated to the objects/shapes analyzed. More shape measures increase the dimensionality of the space of the feature vectors, and consequently, the potential for greater efficiency in shape based tasks (classification, recognition, matching, etc) increases as well. But the number of approaches to design a measure to certain shape property is limited. Thus, the question: *"How else we can increase the power of shape descriptor/measure based tools?"* arises. Here, we have discussed some possibilities. In Sections 2 and 3, we considered area based shape measures (in which all the shape points are used) and show how incorporating a tuning parameter can lead to an infinite family of circularity and ellipticity measures. In Sections 3 and 4, we have illustrated that further improvements can be obtained by assigning multiple shapes to the objects considered. As mentioned, area based measures were used in Section 3, while in Section 4 shape boundaries (i.e. operations on them) were used to allocate the multiple shapes to the objects considered, and then boundary based shape measures were employed.

**Acknowledgements** This work is partially supported by the Ministry of Science of the Republic of Serbia, projects OI174008.

## References


1. Aktaş, M.A., Žunić, J.: Measuring shape ellipticity. In Axel Pinz et al. (eds.): Pattern Recognition - Joint 34th DAGM and 36th OAGM Symposium. Lecture Notes in Computer Science, vol. 7476, pp. 307–316, (2012)
2. Aktaş, M.A., Žunić, J.: A family of shape ellipticity measures for galaxy classification. SIAM J. Imaging Sci. **6**, 765–781 (2013)
3. Arandjelović, O.: Computationally efficient application of the generic shape illumination invariant to face recognition from video. Pattern Recognition **45**, 92–103 (2012)
4. Bazell, D., Peng, Y.: A comparison of neural network algorithms and preprocessing methods for star-galaxy discrimination. The Astrophysical Journal Supplement Series **116**, 47–55 (1998)
5. Bowman, E.T., Soga, K., Drummond, T.: Particle shape characterization using Fourier analysis. Geotechnique **51**, 545–554 (2001)
6. Castro-Bleda, M.J., Boquera, S., Gorbe, J., Zamora, F., Llorens, D., Marzal, A., Prat, F., Vilar-Torres, J.M.: Improving a DTW-Based recognition engine for on-line handwritten characters by using MLPs. In: Proceedings of the 10th International Conference on Document Analysis and Recognition, pp. 1260–1264 (2009)
7. Chang, C.-C. and Lin, C.-J.: LIBSVM: A library for support vector machines. ACM Transactions on Intelligent Systems and Technology **2**, 27 pages (2011)
8. Dorst, L., Smeulders, A.W.M.: Length estimators for digitized contours. Computer Vision, Graphics and Image Processing **40**, 311–333 (1987)
9. Frei, Z., Guhathakurta, P., Gunn, J.E., Tyson, J.A.: A catalog of digital images of 113 nearby galaxies. Astronomical Journal **111**, 174–181 (1996)
10. Gautama, T., Mandić, D.P., Van Hulle, M.M.: Signal nonlinearity in fMRI: A comparison between BOLD and MION. IEEE Trans. Medical Images **22**, 636-644 (2003)
11. Goderya, S.N., Lolling, S.M.: Morphological classification of galaxies using computer vision and artificial neural networks: A computational scheme. Astrophysics and Space Science **279**, 377–387 (2002)
12. Grisan, E., Foracchia, M., Ruggeri, A.: A novel method for the automatic grading of retinal vessel tortuosity. IEEE Trans. Medical Imaging **27**, 310-319 (2008)
13. Guo, Q., Guo, F., Shao, J.: Irregular shape symmetry analysis: Theory and application to quantitative galaxy classification. IEEE Trans. Pattern Anal. Mach. Intell. **32**, 1730–1743 (2010)
14. Han, M.: The luminosity structure and objective classification of galaxies. Astrophysical Journal **442**, 504–522 (1995)
15. Haralick, R.M.: A measure for circularity of digital figures. IEEE Trans. Systems, Man and Cybernetics. **4**, 394–396 (1974)
16. Hu, M.: Visual pattern recognition by moment invariants. IRE Trans. Inf. Theory **8**, 179–187 (1962)
17. Lee D.R., Sallee, T.: A method of measuring shape. Geographical Review **60**, 555–563 (1970)
18. Lekshmi, S., Revathy, K., Prabhakaran Nayar, S.R.: Galaxy classification using fractal signature. Astronomy & Astrophysics **405**, 1163–1167 (2003)
19. Mähönen, P., Frantti, T.: Fuzzy classifier for star-galaxy separation. Astrophysical Journal **541**, 261–263 (2000)
20. Mei, Y., Androutsos, D.: Robust affine invariant region-based shape descriptors: The ICA Zernike moment shape descriptor and the whitening Zernike moment shape descriptor. IEEE Signal Processing Letters **16**, 877–880 (2009)
21. Odewahn, S., Stockwell, E., Pennington, R., Humphreys, R., Zumach, W.: Automated star/galaxy discrimination with neural networks. Astronomical Journal **103**, 318–331 (1992)
22. Otsu, N.: A threshold selection method from gray level histograms. IEEE Trans. Systems, Man and Cybernetics **9**, 62–66 (1979)

23. Pan, F., Keane, M.: A new set of moment invariants for handwritten numeral recognition. In: Proceedings of the International Conference on Image Processing, pp. 154–158 (1994)
24. Proffitt, D.: The measurement of circularity and ellipticity on a digital grid. Pattern Recognition **15**, 383–387 (1982)
25. Ramer, U.: An iterative procedure for the polygonal approximation of plane curves. Computer Graphics and Image Processing **1**, 244–256 (1972)
26. Rahtu, E., Salo, M., Heikkilä, J.: A new convexity measure based on a probabilistic interpretation of images. IEEE Trans. Pattern Anal. Mach. Intell. **28**, 1501-1512 (2006)
27. Rangayyan, R.M, Elfaramawy, N.M., Desautels, J.E.L., Alim, O.A.: Measures of acutance and shape for classification of breast-tumors. IEEE Trans. Medical Imaging **16**, 799–810 (1997)
28. Richardson, E., Werman, M.: Efficient classification using the Euler characteristic. Pattern Recognition Letters **49**, 99–106 (2014)
29. Rosin, P.L.: Measuring shape: Ellipticity, rectangularity, and triangularity. Machine Vision and Applications **14**, 172–184 (2003)
30. Di Ruberto, C., Dempster, A.: Circularity measures based on mathematical morphology. Electronics Letters **36**, 1691–1693 (2000).
31. Rosin, P.L.: Measuring sigmoidality. Pattern Recognition **37**, 1735-1744 (2004)
32. Rosin, P.L., Mumford, C.L.: A symmetric convexity measure. Computer Vision and Image Understanding **103**, 101–111 (2006)
33. Rosin, P.L., Pantović, J., Žunić, J.: Measuring linearity of closed curves and connected compound curves. In: Kyoung Mu Lee et al.: (eds.) 11th Asian Conference on Computer Vision, Lecture Notes in Computer Science, vol. 7726, pp. 310–321, (2012)
34. Rosin, P.L., Žunić, J.: Measuring squareness and orientation of shapes. J. Math. Imaging Vision **39**, 13–27 (2011)
35. Rosin, P.L., Žunić, J.: Orientation and anisotropy of multi component shapes from boundary information. Pattern Recognition **44**, 2147–2160 (2011)
36. Stojmenović, M., Nayak, A., Žunić, J.: Measuring linearity of planar point sets. Pattern Recognition **41**, 2503-2511 (2008)
37. Teja, S.P., Namboodiri, A.M.: A ballistic stroke representation of online handwriting for recognition. In: Int. Conf. on Document Analysis and Recognition, pp. 857-861 (2013)
38. Tool, A.Q.: A method for measuring ellipticity and the determination of optical constants of metals. Phys. Rev. (Series I) **31**, 1–25 (1910)
39. Wang, B.: Shape retrieval using combined Fourier features. Optics Communications **284**, 3504–3508 (2011)
40. Žunić, J., Kakarala, R., Aktaş, M.A.: Elliptical shape signature. Submitted.
41. Žunić, J., Martinez-Ortiz, C.: Linearity measure for curve segments. Applied Mathematics and Computation **215**, 3098-3105 (2009)
42. Žunić, D., Žunić, J.: Shape ellipticity from Hu moment invariants. Applied Mathematics and Computation **226**, 406–414 (2014)
43. Žunić, J., Hirota, K., Rosin, P.L.: A Hu moment invariant as a shape circularity measure. Pattern Recognition **43**, 47–57 (2010)
44. Žunić, J., Rosin, P.L.: Rectilinearity measurements for polygons. IEEE Trans. Pattern Anal. Mach. Intell. **25**, 1193–1200 (2003)
45. Žunić, J., Rosin, P.L.: A new convexity measurement for polygons. IEEE Trans. Pattern Anal. Mach. Intell. **26**, 923–934 (2004)
46. Žunić, J., Rosin, P.L.: Convexity measure for shapes with partially extracted boundaries. Electronics Letters **43**, 380–382 (2007)

# Index

boundary simplification, 12

ellipticity measure, 7

galaxy classification, 7
geometric moment invariants, 2

mamography, 3
measure behavior tuning parameter, 3
MPEG-7 CE-1, 12
multiple shapes, 7

NGC - galaxy images catalog, 7

shape, 2
shape circularity measure, 3
shape descriptor, 2
shape measure, 2

thresholding, 7

UJI Pen character set, 12